J Mater Sci (2014) 49:62–69
DOI 10.1007/s10853-013-7650-9

Phase transition behavior and high piezoelectric properties in lead-free $BaTiO_3$–$CaTiO_3$–$BaHfO_3$ ceramics

Dali Wang · Zhaohua Jiang · Bin Yang · Shantao Zhang · Mingfu Zhang · Feifei Guo · Wenwu Cao

Received: 8 April 2013 / Accepted: 5 August 2013 / Published online: 4 September 2013

Abstract The transition behavior, structural changes, and electric properties of lead-free $(1-x)Ba(Hf_{0.16}Ti_{0.84})O_3$–$x(Ba_{0.70}Ca_{0.30})TiO_3$ (BCHT) ceramics fabricated by the conventional solid-state reaction method are investigated in this study. A complete phase diagram of BCHT system has been proposed based on their dielectric behavior. It is found that BHCT ceramics undergo a complicated phase evolution, driven by Ca and Hf contents. The results clearly demonstrate that high electric properties are achieved in the ferroelectric orthorhombic–tetragonal phase boundary near the composition with $x = 0.48$, which could be adjusted by the contents of Ca and Hf in the composition. The optimum composition shows enhanced properties with dielectric constant $\varepsilon_r = 2889$ (at room temperature, 1 kHz), high piezoelectric coefficient $d_{33} = 410$ pC/N, and electromechanical coupling factor $k_p = 0.47$, and a relative high Curie temperature of 106 °C. This investigation yields a sight to understand different phase transition mechanisms of enhanced piezoelectricity for the system.

D. Wang · Z. Jiang
School of Chemical Engineering and Technology, Harbin Institute of Technology, Harbin 150001, People's Republic of China

D. Wang
College of Sciences, Yanbian University, Yanji 133002, People's Republic of China

B. Yang (✉) · F. Guo · W. Cao
Condensed Matter Science and Technology Institute, Harbin Institute of Technology, Harbin 150001, People's Republic of China
e-mail: binyang@hit.edu.cn

S. Zhang
Department of Materials Science and Engineering & National Laboratory of Solid State Microstructures, Nanjing University, Nanjing 210093, People's Republic of China

M. Zhang
Center for Composite Materials, Harbin Institute of Technology, Harbin 150001, People's Republic of China

W. Cao
Materials Research Institute, The Pennsylvania State University, University Park, PA 16802, USA

Introduction

Lead-based piezoelectric ceramics represented by $Pb(Zr_{1-x}Ti_x)O_3$ (PZT) are dominant for commercial electronic devices due to their superior dielectric and piezoelectric properties [1]. However, the commercial manufacture and application of PZT have recently been restricted because of the Pb toxicity, PbO volatility, and its hazardous effect on the environment [2]. Therefore, the need to reduce environmental contamination by lead-based materials has given a boost to searching for lead-free piezoelectric materials to replace PZT [3, 4]. Among the lead-free compositional families, the titanate perovskite-based piezoceramics, mainly including $BaTiO_3$, $Bi_{0.5}Na_{0.5}TiO_3$, $Bi_{0.5}K_{0.5}TiO_3$, and their solid solutions, are one of the most extensively studied piezoelectric materials [5–9].

Recently, high piezoelectric performance lead-free $(BaCa)(B'Ti)O_3$ (BCB'T, $B' = Zr$, Sn) systems were designed on the same fundamental basis as PZT, which form a rhombohedral–tetragonal morphotropic phase boundary (MPB) characterized by the existence of a triple point [10, 11]. High piezoelectric coefficient of 300–600 pC/N in those systems was obtained for their optimal composition. Large piezoelectric response suggests that they might be the promising alternatives to lead-based piezoelectric materials; the relationship between ferroelectric phase configuration

and its properties were reported [12, 13]. However, the reported systems have relatively low Curie temperatures (T_C); for example, the T_C of BCB′T (B′ = Sn, Hf) is only about ~89 °C, which limits their practical application [11, 14]. That means further improving the T_C and determining the phase transition of these systems might be interesting and necessary.

On the other hand, according to the phase diagrams for $Ba(Ti_{1-x}Hf_x)O_3$ as shown in Fig. 1a, the compositions in the region of $0.10 < x \leq 0.22$ show stable rhombohedral phase at room temperature [15]. The Ti-substitution by Hf^{4+} lowers T_C of $Ba(Ti_{1-x}Hf_x)O_3$ system, pushes both the rhombohedral–orthorhombic transition temperature T_{R-O} and the orthorhombic–tetragonal transition temperature T_{O-T} to higher temperature, leading to the disappearance of T_{R-O} when x reaches 0.16, for which the T_C corresponds to a transition from rhombohedral to cubic near 60 °C. While according to the phase diagrams for $(Ba_{1-x}Ca_x)TiO_3$, the composition with $x < 0.25$ shows stable tetragonal phase at room temperature [16]. Furthermore this system has a solubility limit with $x = 0.23$, and the material becomes tetragonal and orthorhombic diphase coexistence for $x = 0.23$–0.90, and a pure orthorhombic phase for $x = 0.93$–1.0, respectively [17]. Opposite to Ti-substitution, Ba-substitution by Ca^{2+} strongly lowers the T_{O-T} and T_{R-O}, only causes a negligible effect in the T_C for $(Ba_{1-x}Ca_x)TiO_3$, and thus improves the temperature reliability of piezoelectric property [18].

Generally, properties of piezoelectric ceramics can be improved by compositional engineering, where the composition of ceramics is tuned to the proximity with a structural instability at phase transition boundaries such as polymorphic phase transition (PPT) or MPB. The electromechanical response can be enhanced in these regions, which is related to this phase transition. So, it is reasonable that rhombohedral–tetragonal MPB may exist in lead-free $Ba(Hf_{0.16}Ti_{0.84})O_3$–$(Ba_{0.70}Ca_{0.30})TiO_3$ system at room temperature. In addition, it is well-known that in ferroelectric ABO_3 perovskites, the substitution of B cation by another one of the same chemical group can strongly alter its electric properties. Accordingly, it is anticipated that the $Ba(Hf_{0.16}Ti_{0.84})O_3$–$(Ba_{0.70}Ca_{0.30})TiO_3$ system may have excellent piezoelectric properties.

In the present work, ceramics of $(1-x)Ba(Hf_{0.16}Ti_{0.84})O_3$–$x(Ba_{0.70}Ca_{0.30})TiO_3$ (BCHT) ($x = 0.20$, 0.28, 0.45, 0.48, 0.50, 0.52, 0.55, 0.60, 0.65, and 0.80), as indicated by the black dots in Fig. 1b, were prepared. The composition-dependent phase behavior and electric properties were investigated systematically for searching for high-performance lead-free piezoelectric materials as well as expanding the range of the lead-free BCB′T systems.

Experimental procedure

The BCHT ($x = 0.20$, 0.28, 0.45, 0.48, 0.50, 0.52, 0.55, 0.60, 0.65, and 0.80) piezoceramics were prepared by solid-state reaction method. $BaCO_3$ (99.0 %), $CaCO_3$ (99.0 %), HfO_2 (99.99 %), and TiO_2 (99.0 %) were chosen as starting raw materials. For each composition, the oxides and carbonates were weighed according to the stoichiometric ratio of BCHT ceramics. After being ball-milled in alcohol for 24 h using agate balls in planetary mill, the slurries were dried, and then calcined at 1350 °C for 4 h. The calcined powders were subsequently ball-milled again in alcohol for 24 h to obtain homogeneous powder. The powders were pressed into green disks with a diameter of 13 mm using 5 % polyvinyl alcohol as the binder. Following a 550 °C binder burnout, the disks were sintered in covered alumina crucibles at 1480 °C for 3 h. The crystal

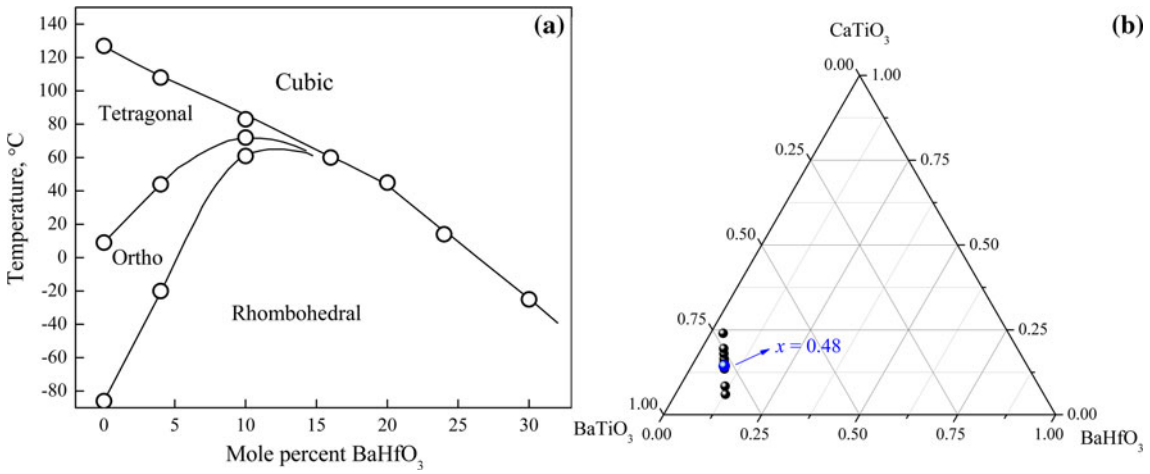

Fig. 1 **a** $BaTiO_3$–$BaHfO_3$ phase diagram re-drawn as proposed in [15]. **b** Schematic representation of the $BaTiO_3$–$CaTiO_3$–$BaHfO_3$ ternary diagram (the studied compositions are indicated by the *dots*)

structures and the morphology of the ceramics were characterized by powder X-ray diffraction (XRD, Rigaku D/max 2400 X-ray diffractometer) with a Cu Kα radiation and scanning electron microscopy (SEM, Quanta 200FEG), respectively. For electrical measurements, silver paste was coated on both sides of the samples as the electrodes and fired at 550 °C for 40 min. Relative dielectric constant (ε_r) and loss tangent (tan δ) as a function of temperature and frequency were measured with a precision impedance analyzer (HP4294A). Polarization–electric field (*P*–*E*) loops and the strain–electric field (*S*–*E*) curves were measured by Precision premier II comprehensive ferroelectric analyzer (Radiant Tech. USA). For the measurement of piezoelectric properties, samples were poled for 40 min at 25 °C under an electric field of 35 kV/cm. The piezoelectric coefficient (d_{33}) was measured at room temperature using a quasi-static d_{33} meter (ZJ-4A, Institute of Acoustics, Chinese Academy of Sciences). The planar electromechanical coupling factors (k_p) and mechanical quality factor (Q_m) were calculated according to the IEEE standard, by using the resonance and antiresonance frequencies, obtained from an HP4294A impedance phase-gain analyzer.

Results and discussion

The XRD patterns of the BCHT ceramics at room temperature are shown in Fig. 2a. All the samples show pure perovskite structure without detectable second phases. The detailed XRD patterns in the 2θ range of 44°–47° and 82°–85° are plotted in Figs. 2b, c. It is observed in Fig. 2c that the diffraction peaks tend to shift to higher angle with increasing *x*, showing a contraction of the unit cell volume and development of strain in the materials [19]. This might be attributed to the radii of the A- and B-site ions in the system. The ionic radius of Ca^{2+} (1.34 Å) and Ti^{4+} (0.605 Å) are smaller than those of Ba^{2+} (1.61 Å) and Hf^{4+} (0.71 Å), leading to the decrease of lattice parameters with increasing *x* [20]. According to the peak splitting of the (200) reflection, the sample with $x = 0.80$, denoted as $(Ba_{0.76}Ca_{0.24})(Hf_{0.032}Ti_{0.968})O_3$, exhibits tetragonal symmetry ($a = 3.9682$ Å, $c = 4.0048$ Å), in which XRD data were fitted to obtain its lattice parameters. Tetragonal and orthorhombic diphase coexistence is not found in this composition, which is the solubility limit with Ba-substitution by Ca^{2+} during synthesis of ceramics [17, 19]. The composition with $x = 0.20$ is stabilized into rhombohedral symmetry ($a = 4.0218$ Å, $\alpha = 89.99$), which is characterized by single (200) peaks at around 2θ of 45° and splitting of the (222) peaks at around 2θ of 83° in Fig. 2c. Attention should be paid to that the structure pass through splitting of the (222) peaks at around 2θ of 83° to merging of the peak, from $x = 0.20$ to $x = 0.45$, and from $x = 0.45$ to $x = 0.80$, respectively. The BCHT ceramics at $x = 0.45$ possess orthorhombic phase, which is characterized by (200) and (222) peaks at around 2θ of 45° and 83°. The change indicates that the composition starts to approach a phase boundary region from orthorhombic phase side after going through rhombohedral phase. By considering the above composition-dependent XRD profiles and following electrical measurements, a phase boundary region between the T–O phase is identified near $x = 0.48$ at room temperature. This T–O phase boundary is different from the previously reported T–R phase boundary near room temperature in this system. This suggests that their different Hf contents in the end of BHT may have a significant impact for the phase boundary near room temperature [14]. In the XRD pattern it is interesting to know about the change in microstrain with changing composition. As presented in Fig. 2d, the lattice strain gradually increases from $x = 0.20$ to $x = 0.48$ and becomes maximum at $x = 0.48$, which might be generated due to the interacting orthorhombic and tetragonal phases in the vicinity of the O–T phase boundary [21].

The SEM micrographs of all the compositions are shown in Fig. 3. The corresponding average grain size d_{av}, which have been calculated from ceramics using the linear intercept method are plotted in Fig. 4. The BCHT ceramic with $x = 0.20$ shows an inhomogeneous grain distribution in which the large one is approximately 29 μm and the small grain is only 4 μm. When $x = 0.45$–0.50, the microstructure becomes more homogeneous, in which the small grains grow close to the big ones. However, the microstructure of ceramics with *x* increasing from 0.52 to 0.80 is inhomogeneous again. Such evolution in grain size may be responsible for the change of interface atomic structure or grain boundary structure caused by Hf and Ca substitution, which significantly affects the microstructure evolution during ceramics sintering [22]. The corresponding varying trend of the average grain size with $x = 0.20$–0.65 is shown in Fig. 4. It is interesting to note that average grain size gradually decreases from $x = 0.20$ to $x = 0.48$, and becomes minimum about 10.9 μm, and then increases up to $x = 0.65$. The average grain size with $x = 0.80$ is not obtained by the linear intercept method for its obscure grain boundary. It is expected that the ceramic possessing clear grain boundary and more homogenous microstructure is advantageous to achieve excellent electrical properties.

To reveal the phase transition behavior, temperature-dependent dielectric measurements were carried out in the range of −80 to 200 °C. The phase diagram of the system is plotted based on the dielectric measurement results, as shown in Fig. 5a. The typical frequency-dependent dielectric constants measured at various frequencies for the composition with $x = 0.20$, 0.28, 0.48, and 0.80 are shown in Fig. 5b. As can be seen, the dielectric constant shows

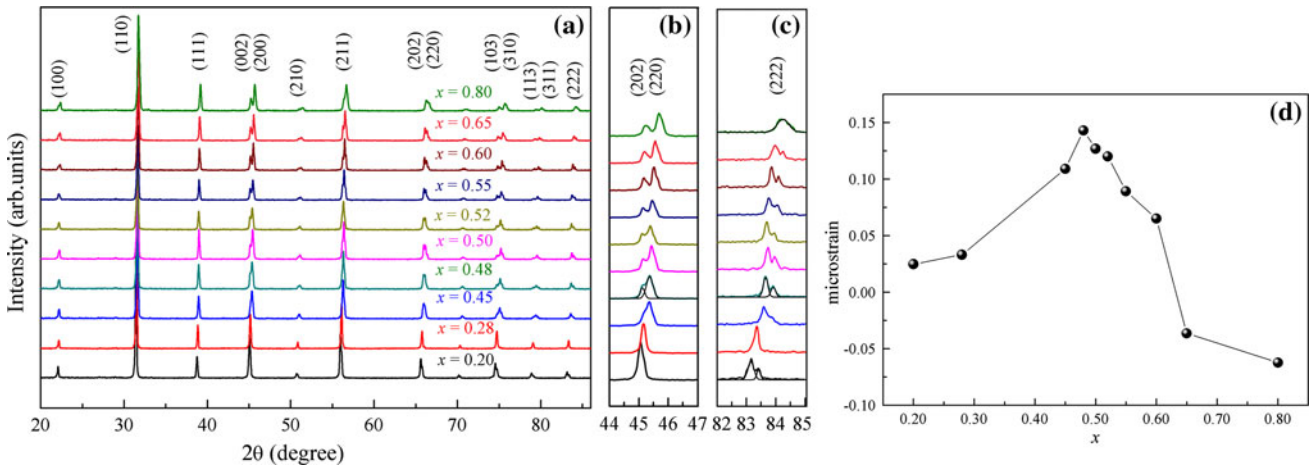

Fig. 2 **a** The room-temperature XRD patterns of the ceramics, **b**, **c** detailed composition-dependent XRD patterns, **d** the lattice strain as the function of composition

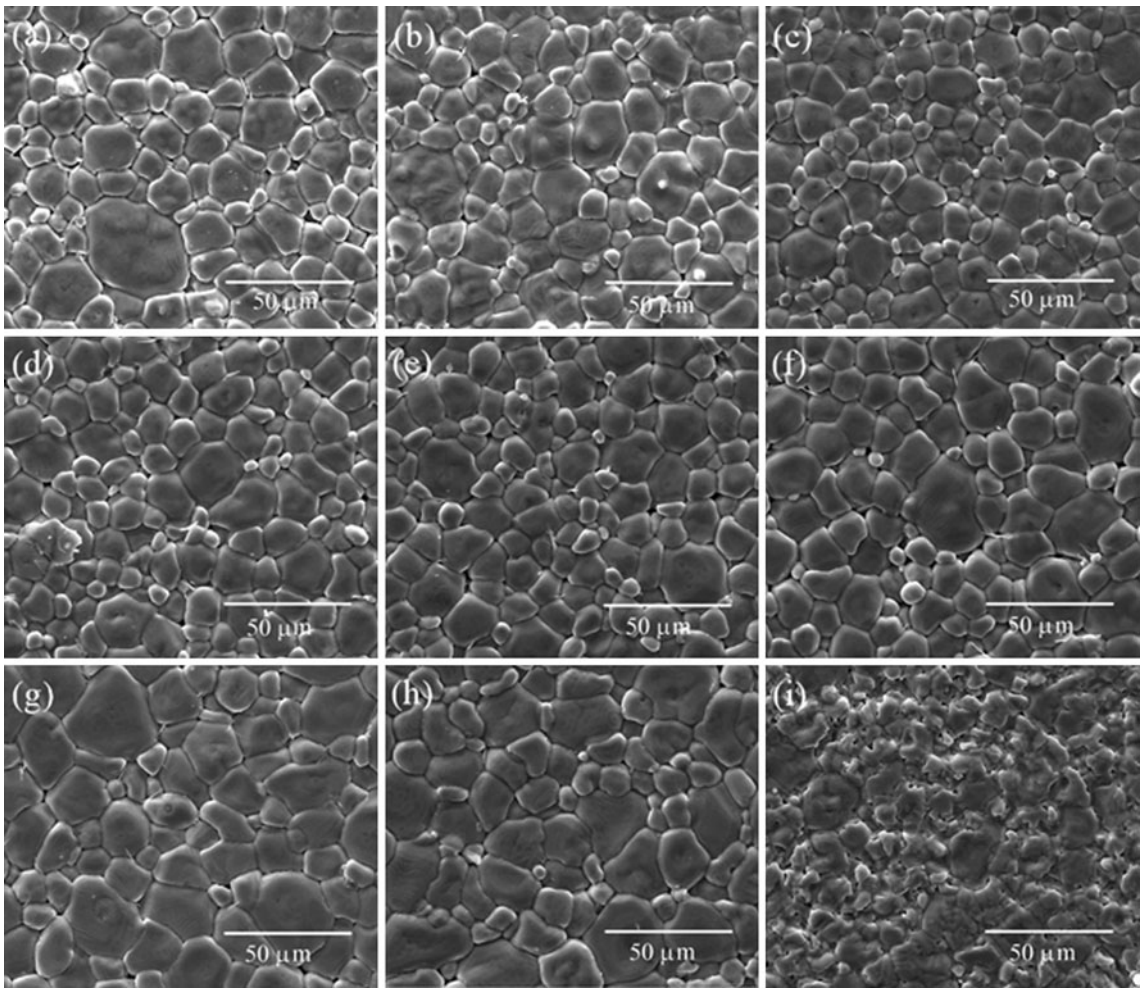

Fig. 3 Microstructures of BCHT ceramics: **a** $x = 0.20$, **b** $x = 0.28$, **c** $x = 0.45$, **d** $x = 0.48$, **e** $x = 0.50$, **f** $x = 0.55$, **g** $x = 0.60$, **h** $x = 0.65$, **i** $x = 0.80$

only slight frequency dependence. For these compositions, the temperature where the dielectric peaks occur is almost independent on frequency. In addition, it is found that for the samples with $x = 0.20$ and $x = 0.80$, the materials pass directly from rhombohedral to cubic phase at 75 °C, and from tetragonal to cubic phase at 119 °C, respectively. It is

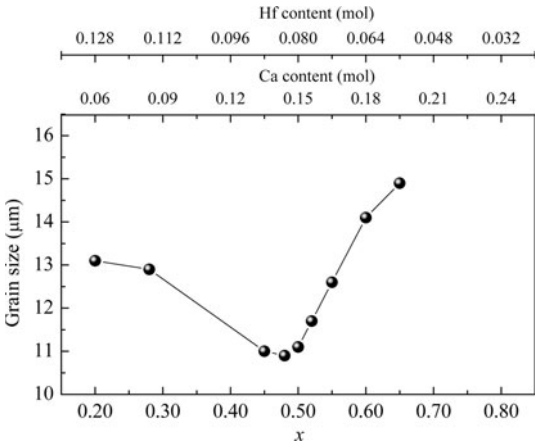

Fig. 4 The average grain size as the functions of composition

a result from that competition between Hf and Ca ions which pushes both the T_{R-O} and the T_{O-T} to higher or lower temperature, leading to the disappearance of T_{R-O} with $x = 0.20$ composition, or the appearance of T_{R-O} with $x = 0.80$ composition in the outside measured temperature range. For $x = 0.28$, the three phase transitions merge together in one broad peak for forming a phase convergence region, as is similar to that of BCZT systems [23]. This composition exhibits the highest permittivity peak at T_C compared with that of other compositions in Figs. 5b, d. This anomaly further supports the existence of the phase convergence region. It should be noted that three dielectric anomalies existed for the sample with $x = 0.48$, corresponding to the transition temperatures T_{R-O} and T_{O-T} and Curie temperature T_C, respectively. The composition owns a PPT similar to the phase transitions of the $BaTiO_3$, $Ba(Ti_{1-x}Hf_x)O_3$, and $(Ba_{1-x}Ca_x)TiO_3$ ceramics [15, 16]. The T_{R-O} and T_{O-T} phase transition temperatures are about −5 and 26 °C, respectively, by the first derivative of the dielectric constant for the sample with $x = 0.48$ in Fig. 5c. The T_{O-T} of this composition is very close to room temperature, which may further contribute to the formation of T–O phase coexistence in BHCT ceramics, indicating the possible higher piezoelectric performance of this composition.

The temperature dependence of the dielectric constant at 1 kHz for samples with $x = 0.45$–0.65 are presented in Fig. 5d. It is found that the T_C slightly shifts to a lower temperature, while the T_{O-T} and T_{R-O} go upward with decreasing x. The T_C shift is attributed to the effect of ionic radius, the valence state and the ground state of the substituent ion on B sites [24]. Both the acceptor ion and the presence of oxygen vacancies tend to remove locally the tetragonal symmetry and the ferroelectric state, thus leading to a reduction of T_C. However, in the case of isovalent Hf^{4+} no oxygen vacancies are formed resulting from Ti-substitution by Hf^{4+}, the ferroelectric state is weakly disturbed [25]. Generally, hafnium could restrain the concentration of oxygen vacancies owing to the chemical stability of Hf^{4+} being superior to that of Ti^{4+} [26]. Accordingly, the phenomenon of Curie temperature drop may be attributed to difference of ionic radius, in which the radius of the Hf^{4+} ion is larger than that of the Ti^{4+} ion. Ti-substitution by Hf^{4+} will weaken the bonding force between the B-site ion and the oxygen ion of the ABO_3 perovskite structure, meanwhile leading to a weaker distortion of the octahedron [27].

The composition dependence of room-temperature dielectric constant and loss tangent of this system is illustrated in Fig. 5e. With increasing x, the loss tangent begins to increase slightly to maximum at $x = 0.28$ and then decreases gradually, in which the variation of room-temperature loss tangent in this study might be dominantly due to that presence position of the dielectric loss peaks related with the composition change [28]. Meanwhile the relative dielectric constant reaches the maximum for the composition with $x = 0.48$. The dielectric constant and loss tangent values of this phase boundary composition are 2889 and 0.012 at 1 kHz, respectively. The O–T phase coexistence of this composition should be responsible for its highest relative permittivity.

The room-temperature polarization–electric field (P–E) loops of all samples at a field of 35 kV/cm are shown in Fig. 6a. In agreement with other reported lead-free BCB′T (B′ = Zr, Sn) systems, the P–E loops are well saturated with low coercive fields. The corresponding composition-dependent saturated polarization (P_S), remnant polarization (P_r), and coercive field (E_C) are plotted in Fig. 6b. As can be seen, the P_S and P_r change slightly, reaching the peak values of 16.1 and 7.44 μ C/cm^2 at $x = 0.48$, respectively, and then decrease with further increasing x. It is clear that the change of P_r after $x = 0.48$ is not significant. The coercive field E_C, however, is observed to decrease first with $x = 0.20$–0.28 and then increase from 1.5 to 6.9 kV/cm with increasing x from 0.28 to 0.80. This indicated that the domain switching becomes harder attributing to the increase of the tetragonal phase.

The variations of the piezoelectric coefficient d_{33}, electromechanical coupling factor k_p, and mechanical quality factor Q_m as the function of x are shown in Fig. 7a. It is found that the d_{33}, k_p, and Q_m show strong composition dependence, and the maximum d_{33} and k_p values of 410 pC/N and 0.47, respectively, are obtained in the composition with $x = 0.48$. Moreover, the enhanced piezoelectric properties are considered to be reasonably consistent with coexistence of R-phase and O-phase, and PPT occurring near room temperature should be the origin of this phase coexistence. The composition-induced O–T phase transition causes the instability of the polarization

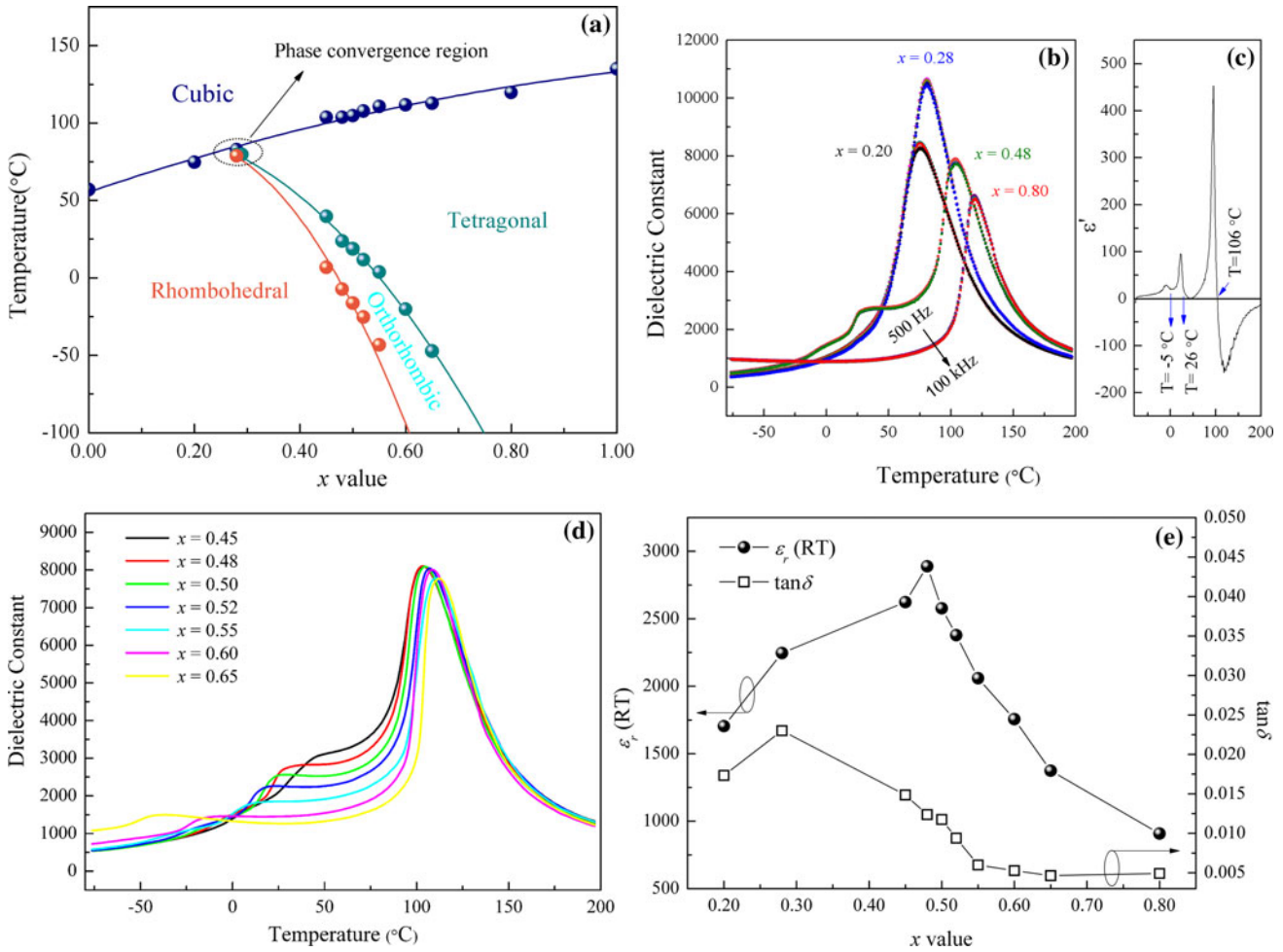

Fig. 5 **a** Phase diagram of the BCHT ceramics. **b** Typical dielectric temperature curves at different frequencies (500 Hz–100 kHz) with $x = 0.20$, 0.28, 0.48, and 0.80. **c** The first derivative of the dielectric constant for the sample with $x = 0.48$. **d** Temperature dependence of relative dielectric constant at 1 kHz with $x = 0.45$–0.65. **e** Composition dependence of room temperature relative dielectric constant at 1 kHz

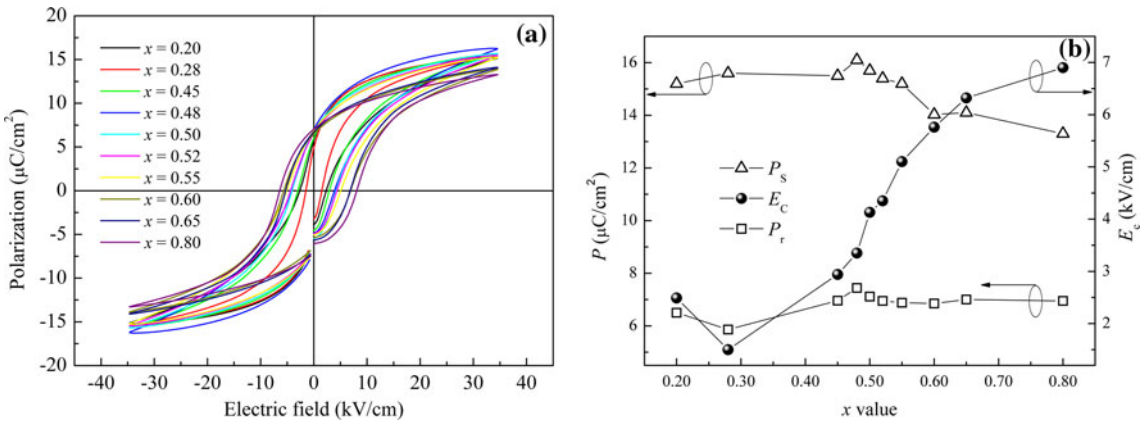

Fig. 6 **a** Ferroelectric hysteresis loops of the composition with $x = 0.48$ and **b** composition-dependent P_s, P_r, and E_C

state, so that the polarization direction can be easily rotated by external stress or electric field, resulting in high piezoelectric performances [29].

All the investigated samples display typical ferroelectric butterfly-shaped bipolar *S*–*E* curves, typical result of the composition with $x = 0.48$ is shown in the inset of Fig. 7b.

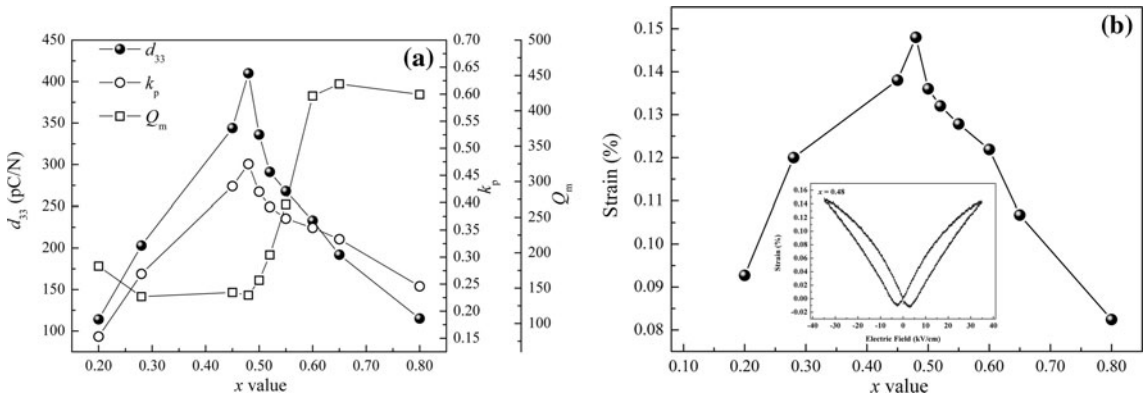

Fig. 7 **a** The piezoelectric coefficient, coupling factor, and mechanical quality factor as the functions of composition. **b** Composition-dependent positive strain as the function of composition at RT. The *inset* depicts the typical bipolar *S–E* field curve of the investigated piezoceramics

For clarifying the composition dependence of *S–E* shape in detail, the maximum positive strain is displayed as a function of x in Fig. 7b. As can be seen, the positive strain value reaches peak values of 0.14 % at $x = 0.48$ with increasing x, which is consistent with the piezoelectric measurements shown in Fig. 4. In addition, it is noted that the above-mentioned enhanced electrical properties for the O–T phase boundary composition with $x = 0.48$ may be relative to its more homogenous microstructure as shown in Fig. 3.

The enhancement of the electric response in BCHT ceramics is achieved by tuning composition. Following this approach the composition of ceramics is tuned to the proximity of a region with a structural instability such as T–O or T–R phase boundary [14]. The system possessing T–O phase boundary shows higher T_C than that possessing T–R phase boundary reported for BHT-50BCT by controlling Hf content in certain range, but it has a lower piezoelectricity similar to other BT-based systems. Such difference is considered to stem from the dissimilar anisotropy for polarization rotation, the different elastic softenings and the different domain wall contributions between T–R and T–O phase boundaries [30].

Conclusions

In summary, lead-free BHCT ceramics were designed and fabricated by the conventional solid-state reaction method. The dependence of phase structure on the composition has been determined by the XRD patterns and the dielectric measurement for all compositions. The temperature–composition phase diagram of the system has been proposed based on the dielectric measurement results. It is found that BHCT ceramics undergo a complicated phase evolution, driven by Ca and Hf contents. The phase transition behavior confirms the formation of a phase boundary between the ferroelectric O-phase and T-phase near the composition with $x = 0.48$. The composition-dependent electrical properties of this system have been investigated systematically. The optimal composition exhibits high piezoelectric coefficient of $d_{33} = 410$ pC/N, the electromechanical coupling factor $k_p = 0.47$ at room temperature, and the relative high Curie temperature of 106 °C which is comparative with similar systems. This investigation yields a sight to understand different phase transition mechanisms of enhanced piezoelectricity for the system.

Acknowledgements This work was supported by the National key Basic Research Program of China (973 Program, 2013CB632900), the Key Technologies R&D Program of China under Grant No. 2013BAI03B06, and the National Nature Science Foundation of China (10704021, 51102062, and 11174127).

References

1. Haertling G (1999) J Am Ceram Soc 82:797
2. Rödel J, Jo W, Seifert K, Anton E, Granzow T (2009) J Am Ceram Soc 92:1153
3. Li J, Wang K, Zhang B, Zhang L (2006) J Am Ceram Soc 89:706
4. Zhang S, Kounga A, Aulbach E, Granzow T, Jo W, Kleebe H, Rödel J (2008) J Appl Phys 103:1–034107
5. Ni F, Luo L, Pan X, Zhang Y, Chen H (2012) J Mater Sci 47:3354. doi:10.1007_s10853-011-6177-1
6. Chung H, Yang C, Chen K, Diao C (2009) Ferroelectrics 385:89
7. Dai Y, Zhang S, Shrout T, Zhang X (2010) J Am Ceram Soc 93:1108
8. Xu C, Lin D, Kwok K (2008) Solid State Sci 10:934
9. Wang F, Xu M, Leung C, Tang Y, Wang T, Chen X, Shi W (2012) J Mater Sci 47:282
10. Liu W, Ren X (2009) Phys Rev Lett 103:257602
11. Xue D, Zhou Y, Bao H, Gao J, Zhou C, Ren X (2011) Appl Phys Lett 99:122901
12. Damjanovic D, Biancoli A, Batooli L, Vahabzadeh A, Trodahl J (2012) Appl Phys Lett 100:192907
13. Su S, Zuo R, Lu S, Xu Z, Wang X, Li L (2011) Curr Appl Phys 11:120
14. Zhou C, Liu W, Xue D, Ren X, Bao H, Gao J, Zhang L (2012) Appl Phys Lett 100:222910

15. Payne W, Tennery V (1965) J Am Ceram Soc 48:413
16. Mitsui T, Westphal W (1961) Phys Rev 124:1354
17. Wang X, Yamada H, Xu C (2005) Appl Phys Lett 86:022905
18. Berlincourt DA, Kulesar F (1952) J Acoust Soc Am 24:709
19. Panigrahi M, panigrahi S (2010) Phys B 405:1787
20. Shannon R (1976) Acta Cryst A 32:751
21. Frantti J, Eriksson S, Ivanov H, Lantto V, Lappalainen M, Kakihana (2004) J Eur Ceram Soc 24:1141
22. Ye S, Fuh J, Lu L (2012) J Alloys Compd 541:396
23. Keeble D, Benabdallah F, Thomas P, Maglione M, Kreisel J (2013) Appl Phys Lett 102:092903
24. Hagemann H, Ihrig H (1979) Phys Rev B 20:3871
25. Hansen P, Hennings D, Schreinemacher H (1998) J Electroceram 2:85
26. Chen J, Fu C, Cai W, Chen G, Ran S (2012) J Alloys Compd 544:82
27. Kuang S, Tang X, Li L, Jiang Y, Liu Q (2009) Scripta Mater 61:68
28. Cai W, Fu C, Gao J, Lin Z, Deng X (2012) Ceram Int 38:3367
29. Damjanovic D (2005) J Am Ceram Soc 88:2663
30. Yao Y, Zhou C, Lv D, Wang D, Wu H, Yang Y, Ren X (2012) Europhys Lett 98:27008